LETTERS

Lower-crustal intrusion on the North Atlantic continental margin

R. S. White[1], L. K. Smith[1]†, A. W. Roberts[1], P. A. F. Christie[2], N. J. Kusznir[3] & the rest of the iSIMM Team‡

When continents break apart, the rifting is sometimes accompanied by the production of large volumes of molten rock[1–3]. The total melt volume, however, is uncertain, because only part of it has erupted at the surface. Furthermore, the cause of the magmatism is still disputed—specifically, whether or not it is due to increased mantle temperatures. We recorded deep-penetration normal-incidence and wide-angle seismic profiles across the Faroe and Hatton Bank volcanic margins in the northeast Atlantic. Here we show that near the Faroe Islands, for every 1 km along strike, 360–400 km^3 of basalt is extruded, while 540–600 km^3 is intruded into the continent–ocean transition. We find that lower-crustal intrusions are focused mainly into a narrow zone ~50 km wide on the transition, although extruded basalts flow more than 100 km from the rift. Seismic profiles show that the melt is intruded into the lower crust as sills, which cross-cut the continental fabric, rather than as an 'underplate' of 100 per cent melt, as has often been assumed. Evidence from the measured seismic velocities and from igneous thicknesses are consistent with the dominant control on melt production being increased mantle temperatures, with no requirement for either significant active small-scale mantle convection under the rift or the presence of fertile mantle at the time of continental break-up, as has previously been suggested for the North Atlantic Ocean[4–6].

The Hatton Bank continental margin in the northeast Atlantic was one of the first where high-velocity (>7.2 km s^{-1}) lower crust was identified as being caused by magmatism during continental break-up above a mantle thermal anomaly[7]. High-velocity lower crust is now known to be ubiquitous on volcanic continental margins, including all those in the northern North Atlantic[3–11]. Although the high-velocity section is commonly referred to as 'underplated' igneous material, we show from seismic reflection profiles and tomographic velocity inversions of wide-angle data that on the continent–ocean transition (COT) it actually represents continental crust intruded by sills. Failure to recognize the influence of residual continental crust on the lower-crustal seismic velocity may be responsible for interpretations that infer lower mantle temperatures, active small-scale mantle convection and the presence of fertile mantle during continental break-up[4–6].

We report results from two iSIMM (integrated Seismic Imaging and Modelling of Margins)[12–14] transects that imaged the reflectivity and

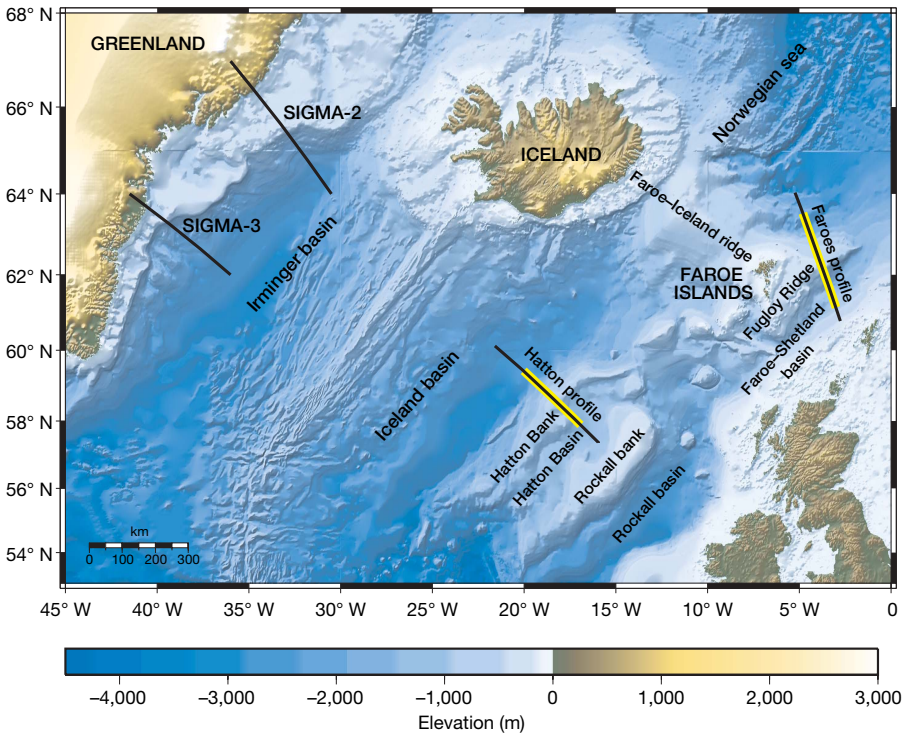

Figure 1 | Location of seismic profiles across the North Atlantic rifted continental margins[4,5,13,14]. The portions of Hatton and Faroes profiles highlighted in yellow are shown in Fig. 2.

[1]Bullard Laboratories, University of Cambridge, Madingley Road, Cambridge CB3 0EZ, UK. [2]Schlumberger Cambridge Research, High Cross, Madingley Road, Cambridge CB3 0EL, UK. [3]Department of Earth Sciences, University of Liverpool, Liverpool L69 3BX, UK. †Present address: BP, Burnside Road, Farburn Industrial Estate, Dyce, Aberdeen AB21 7PB, UK. ‡A list of participants and their affiliations appears at the end of the paper.

velocity structure of the COT. The profiles are 800 km apart (Fig. 1), but exhibit remarkably similar structures. One profile crosses the Hatton margin[7,14], the other crosses the margin near the Faroe Islands, close to the centre of the inferred mantle thermal anomaly[1,8,13]. Both are in similar geological settings, with late Mesozoic failed rifts (the Hatton and Faroe–Shetland basins) separated from the new ocean basins by continental blocks (Hatton Bank and the Fugloy Ridge). We recorded multiple crustal refractions and wide-angle Mohorovičić discontinuity (Moho) reflections, from which two-dimensional velocity models were derived by tomographic inversions (Fig. 2a, b).

A seismic reflection profile along the Faroes line imaged the internal structure of both the extrusive basalt flows and the intruded lower crust (Fig. 2c). Post-rift sediments less than 1 km thick (purple and blue in Fig. 2), lie above basalt flows with seismic velocities that increase downwards from ~4.5 km s^{-1} to ~5.5 km s^{-1}, probably owing to a decrease in weathering and the closure and infilling of cracks and voids with secondary minerals[15]. The basalts reach 7 km thick at the COT and extend ~100 km landward before feathering out in the Faroe–Shetland trough[16]. The base of the basalt flows on the Faroes margin is marked by lower-velocity material (~4.2–4.5 km s^{-1}), presumed to consist of hyaloclastites and early Palaeocene sediments intruded by sills (Fig. 2b, c and Fig. 3b; see also Supplementary Figs 6 and 7, which show examples of the constraints from wide-angle ocean bottom seismometer (OBS) data used to model the low velocity zone). Over the COT, seaward-dipping reflector sequences (SDRS) are imaged well (Fig. 2c, and enlargement in Supplementary Fig. 8). Their arcuate shape results from crustal stretching and subsidence contemporaneous with basalt extrusion, and though the present dip is seaward, the lava was emplaced by landward flow from a subaerial rift[17]. Landward of the COT, flow across the continental hinterland creates layered sub-horizontal basalts.

In the lower crust of the COT, strong sub-horizontal reflections interpreted as sills intrude the dipping fabric of the Archaean continental crust (Fig. 2c). On a depth section the continental fabric dips over 10° seaward, while the intersecting sills exhibit variable dips mostly within ±5° of the horizontal, consistent with the variable 'saucer' shapes of sills imaged in sedimentary sections. Synthetic seismogram modelling suggests that the reflections probably represent complex interference patterns from multiple sills, rather than from individual intrusive bodies[18]. They are most prominent at mid-crustal depths, with the reflectivity decreasing downwards as the proportion of intruded material in the crust increases. On the adjacent Faroe–Iceland ridge, with fully igneous crust that is 30–35 km thick[19], little lower-crustal layering is imaged, despite massive melt intrusion[20]. The absence of layering on the Faroe–Iceland ridge and in the deepest part of the COT crust may be explained by low impedance contrasts between sills injected into an igneous section with the same composition[20], in contrast to their injection into the remnant continental crust of the COT at shallower levels.

The COT region with lower-crustal sills coincides with increased seismic velocities compared to the adjacent continental crust of Hatton Bank and the Fugloy Ridge (Fig. 2a, b). The highest lower-crustal velocities are not reached until the onset of mature seafloor spreading, which is marked by linear magnetic anomalies and coincides with the termination of SDRS and submarine rather than subaerial volcanism[21]. We interpret this oceanic crust as comprising 100% igneous rock with restricted lateral flow, in contrast to the large distances over which subaerial basalts flowed from the COT rift.

If the continental velocity–depth profile is taken as an end-member, while the earliest oceanic crust beyond the termination of the SDRS represents the velocity of the fully igneous crust (Fig. 3a, b), then the lower-crustal igneous volume fraction under the COT can be calculated from the average seismic velocity using a linear mixing law. The total melt volume at the COT on the Faroes profile, including the

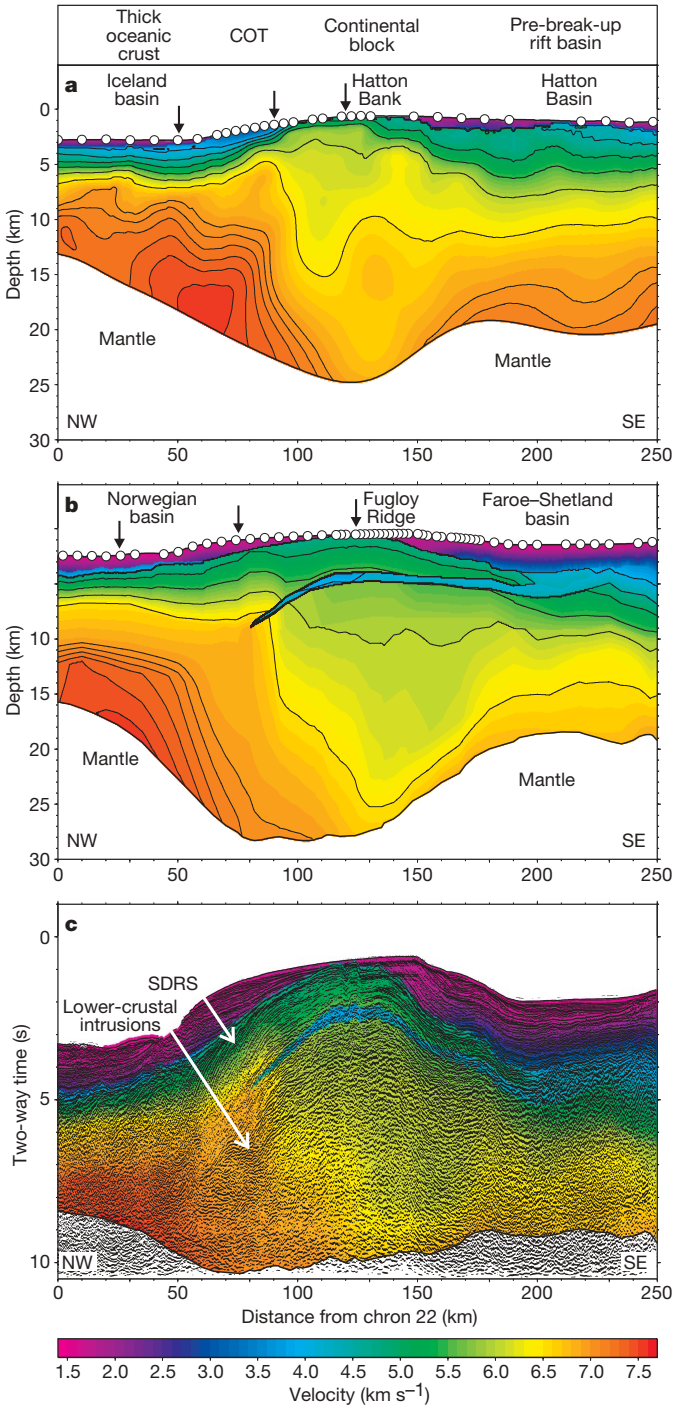

Figure 2 | Seismic velocity profiles. Seismic velocity structure of crust across the continent–ocean transition near Hatton Bank (**a**) and the Faroe Islands (**b**). **c**, Coincident seismic reflection profile across the Faroes margin with velocity field superimposed. Lava flows are imaged as SDRS between 50–90 km along the Faroes profile and as sub-horizontal layered basalts at >90 km. Lower-crustal layering coincident with high (>7.0 km s^{-1}) velocities, caused by igneous intrusions, lies beneath the basalts on the continent–ocean transition, terminating at ~90 km against continental crust with markedly lower velocities. For line locations see Fig. 1. Profiles are aligned with 0 km distance at seafloor spreading magnetic anomaly chron 22. Arrows mark locations of velocity curves shown in Fig. 3. See Supplementary Information for enlargement of COT portion of reflection profile shown in **c**. Reflection profile processing included source designature, multiple suppression and post-stack time migration. Velocities of post-rift Cenozoic sediments (purple) are constrained by semblance move-out analysis of reflections recorded on the hydrophone streamer and sub-sediment crustal velocities are constrained by tomography using wide-angle reflections and diving waves from OBS data (locations shown by white circles at the sea floor). Colour bands are at 0.1 km s^{-1} intervals, with contours above 7.0 km s^{-1} spaced every 0.1 km s^{-1} to highlight the lower-crustal velocity.

extrusive basalts from the reflection image, is about 900–1,000 km^3 per kilometre along strike. The ratio of intruded to extruded igneous rock is 1.5:1, consistent with suggestions on petrological grounds that the intrusive volume must be 'at least as large as the amount of erupted surface lava'[22] and more precise than previous estimates which range from 0.25:1 to 4:1 (ref. 2).

Good velocity and thickness constraints on the igneous component of the crust allow us to address the controversy over whether the large volumes of melt on volcanic margins were produced by rifting above abnormally hot mantle (a 'mantle plume')[1–3,7–9,19], or by active small-scale convection of lower-temperature mantle under the rift, or by melting enriched, more-fertile mantle[4–6]. Increased mantle temperatures cause increased melt thickness h and increased seismic velocity v_P of the igneous rock generated by mantle decompression beneath rifts[1,4–6,23]. On a h–v_P plot (Fig. 3d), the filled circle shows the average for normal oceanic crust[24,25], with the yellow arrow showing the trend predicted for passive decompression melting of normal mantle as its temperature increases. Active mantle upwelling with no temperature change causes increased igneous thickness with little change in seismic velocity, whereas fertile mantle could generate an increase in igneous thickness and a decrease in seismic velocity (solid black arrows in Fig. 3d). Crustal melt fractionation causes the lower-crustal velocity to increase, while melt fractionated deeper in the mantle causes it to decrease (broken black arrows in Fig. 3d)[6]. These effects work in opposite directions, so they may (to first order) cancel one another. The h–v_P curves in Fig. 3d are calculated for primary melt crystallized at the average pressure (230 MPa) and temperature (150 °C) of the lower oceanic crust on our profiles. We follow ref. 6 in using the average lower-crustal velocity as the best available estimate of the primary igneous composition.

The h–v_P data from the oceanic portions of our profiles and from the SIGMA-3 profile on the Greenland margin conjugate to our Hatton profile[5] (Fig. 1) show a clear trend towards normal oceanic crust (filled symbols in Fig. 3c). This trend can be explained solely by passive decompression melting of normal mantle with a temperature decrease of about 75 °C during seafloor spreading after continental break-up. However, the portions of both the Hatton and Faroes profiles with SDRS show trends of decreasing v_P and increasing thicknesses in a landward direction (open symbols in Fig. 3c). At first, this appears to suggest that the mantle temperature was lower (lower v_P) when the SDRS were formed than when the subsequent oceanic crust was generated, with the observed crustal thickness requiring active local convection under the rift at up to ten times the passive upwelling rate[6]. It is also possible that the mantle was more fertile. This is the interpretation of similar h–v_P patterns found for crust beneath SDRS (termed 'transitional crust' on the SIGMA-2

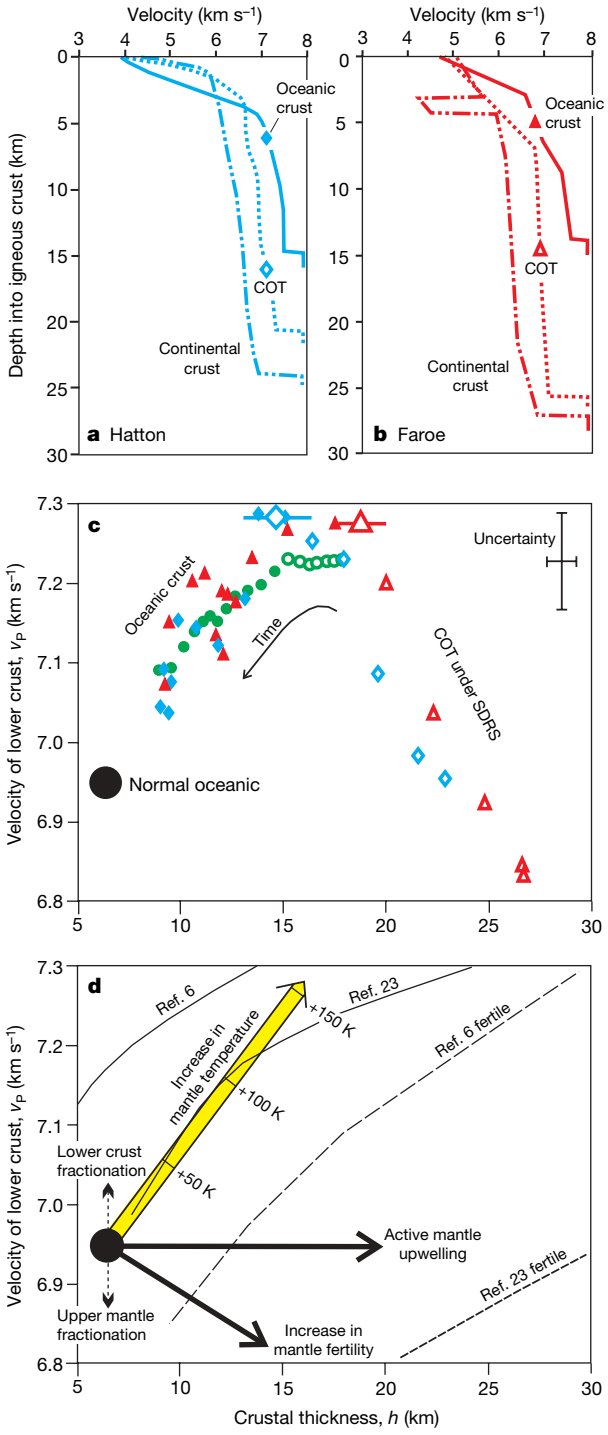

Figure 3 | Crustal velocities and thicknesses. Seismic velocity variation versus depth beneath the base of the sediments at three representative locations: on the oceanic crust, on the COT, and on the continental block of the Hatton Bank profile (**a**) and the Faroe profile (**b**). Locations of velocity curves are shown by arrows on Fig. 2. The oceanic crust and lower continental crust are the two end-members, while the COT crust exhibits lower-crustal velocities intermediate between the two owing to intrusion of continental crust by igneous sills. **c**, Average crustal thickness and lower-crustal velocity calculated every 10 km along the Faroes profile (red triangles), the Hatton profile (blue diamonds), including the oceanward end of our profiles beyond those shown in Fig. 2 (ref. 21), and the conjugate east Greenland SIGMA-3 profile[5] after correction to our reference pressure and temperature (green circles). Filled symbols are from oceanic crust; open symbols are from crust lying on the COT beneath arcuate SDRS. The pair of larger triangle and diamond symbols shows the limits of the total (intrusive plus extrusive) igneous thickness across the Faroes and Hatton COTs, respectively. The extrusive volume is calculated from the seismic reflection images and the intrusive volume is calculated from lower-crustal velocity using a linear mixing law between lower continental crust and fully igneous crust. The standard deviations typical of the data points are shown in the top right corner: the theoretical curves have similar uncertainties. The arrow marked 'time' shows the direction in which the basalts become younger. **d**, Theoretical igneous crustal thickness versus seismic velocity of primary melts generated by passive mantle upwelling under an oceanic rift calculated by refs 6 and 23: solid lines are from normal pyrolitic mantle, and broken lines from fertile mantle. Curves are for a reference pressure of 230 MPa and temperature of 150 °C, which are representative of conditions in the lower-crust of the oceanic data in our results. The filled circle shows the average thickness and lower-crustal velocity of normal oceanic crust[24], after correction for along-segment variation in thickness[25]. The yellow arrow shows the representative trend of changes in h and v_P for passive decompression of normal mantle of increasing temperature, with tick marks approximately every 50 K. Solid arrows show the directions of change in h and v_P at fixed mantle temperature for active mantle upwelling under the rift or an increase in the fertility of the parent mantle. Broken arrows show the effect on the lower-crustal velocity of fractionation in the lower crust or in the upper mantle.

profile[4]) on the conjugate Greenland margin[4–6]. If the lower crust beneath the COT (where the SDRS are observed) comprised 100% igneous material, as the term 'underplated' implies, then this interpretation would be correct. We note that this interpretation introduces other significant difficulties, such as requiring a near-vertical boundary between continental and fully igneous crust at a distance of 90 km on Figs 2b and c, and failing to explain how the SDRS remained elevated and subaerial over the inferred lower-temperature mantle but then subsided and became submarine during seafloor spreading when the inferred mantle temperature was higher.

However, the average h–v_P values for only the igneous component of the COT crust (larger open symbols in Fig. 3c), can be alternatively interpreted as representing melt generated by decompression of hot mantle by lithospheric stretching of the COT before the onset of seafloor spreading. There is the possibility of some trade-off between the assumed velocity of the igneous intrusions under the COT and their thicknesses, which would allow the inference of limited small-scale active convection to generate the melt thickness, but even if this were so, modelling shows that increased mantle temperatures are still required[26]. To first order, the observations for both the Hatton and Faroes profiles can be explained by a model in which the mantle temperature was highest at the start of continental break-up, followed by an approximately 75 °C decrease of mantle temperature over about ten million years of seafloor spreading. This also explains the subaerial elevation of the COT with production of SDRS over the hottest mantle, with a change to submarine seafloor spreading as the mantle temperature decreased after continental break-up. It raises the likelihood that the region of crust with SDRS on the Greenland margin, which is twice as wide as that on the conjugate Hatton margin[5,14], is also underlain by highly stretched continental crust, with initial highly asymmetric stretching similar to that frequently found on non-volcanic margins.

METHODS SUMMARY

Acquisition. Wide-angle data were recorded to ranges >140 km by 85 four-component OBSs spaced at 2–10 km along the profiles, with the seismic source provided by a large-volume (6,360 in^3, 104 litres) airgun array towed at 20 m depth[27] (for data examples see Supplementary Information). The deep-penetration seismic reflection profiles across the Faroes margin used a 48-gun source (10,170 in^3, 167 litres), towed at 18 m depth, and tuned on the bubble so as to produce a broadband signature centred on 9–10 Hz. This low-frequency seismic signal passed through the layered basalts, which severely attenuate higher frequencies[28]. The 12,000 m streamer was towed at 18 m depth so as to enhance its low-frequency response.

Reflection seismic processing. The processing included source signature deconvolution, model-independent multiple attenuation, cascaded Radon demultiple steps and integrated velocity analysis with OBS wide-angle tomography.

Velocity structure. Velocities within the water column were measured by velocimeter and calculated from the temperature measured by disposable bathy-thermographs. Sediment velocities were calculated from semblance analysis of wide-angle reflections on the streamer data. Travel times of individual traces were picked from the vertical component geophone OBS data, and used to map the crustal velocity structure by first-arrival seismic tomography[29], then refined by ray-tracing inversion[30], and for the Hatton profile by joint reflection and refraction tomographic inversion[4]. On the Faroes profile we fitted 15,531 diving waves and 9,865 Moho reflections to within the picking error uncertainties; on the Hatton profile we fitted 17,639 diving waves and 7,850 Moho reflections. Uncertainties in the velocities were estimated by making multiple inversions with 100 randomized starting velocity models: velocities are generally constrained to better than 0.1 km s^{-1} and Moho depths to 1 km (see Supplementary Information for examples of data and model uncertainty). The top of the oceanic lower crust is marked by the velocity inflection at 6.7 km s^{-1} (Fig. 3a and b).

Full Methods and any associated references are available in the online version of the paper at www.nature.com/nature.

Received 24 October 2007; accepted 8 January 2008.

1. White, R. & McKenzie, D. Magmatism at rift zones: The generation of volcanic continental margins and flood basalts. *J. Geophys. Res.* **94,** 7685–7729 (1989).
2. Coffin, M. F. & Eldholm, O. Large igneous provinces: crustal structure, dimensions, and external consequences. *Rev. Geophys.* **32,** 1–36 (1994).
3. Eldholm, O. & Grue, K. North Atlantic volcanic margins: dimensions and production rates. *J. Geophys. Res.* **99,** 2955–2988 (1994).
4. Korenaga, J. *et al.* Crustal structure of the southeast Greenland margin from joint refraction and reflection seismic tomography. *J. Geophys. Res.* **105,** 21591–21614 (2000).
5. Hopper, J. R. *et al.* Structure of the SE Greenland margin from seismic reflection and refraction data: Implications for nascent spreading center subsidence and asymmetric crustal accretion during North Atlantic opening. *J. Geophys. Res.* **108** (B5), 2269–2291 (2003).
6. Korenaga, J., Kelemen, P. B. & Holbrook, W. S. Methods for resolving the origin of large igneous provinces from crustal seismology. *J. Geophys. Res.* **107** (B9), doi:10.1029/2001JB001030 (2002).
7. White, R. S. *et al.* Magmatism at rifted continental margins. *Nature* **330,** 439–444 (1987).
8. Barton, A. J. & White, R. S. Crustal structure of the Edoras Bank continental margin and mantle thermal anomalies beneath the North Atlantic. *J. Geophys. Res.* **102,** 3109–3129 (1997).
9. Larsen, H. C. & Saunders, A. D. in *Proceedings of the Ocean Drilling Program, Scientific Results* (eds A. D. Saunders, H. C. Larsen & S. W. Wise, Jr) Vol. 152 503–533 (Ocean Drilling Program, College Station, Texas, 1998).
10. Weigel, W. *et al.* Investigations of the east Greenland continental margin between 70° and 72° N by deep seismic sounding and gravity studies. *Mar. Geophys. Res.* **17,** 167–199 (1995).
11. Klingelhöfer, F., Edwards, R. A., Hobbs, R. W. & England, R. W. Crustal structure of the NE Rockall Trough from wide-angle seismic data modelling. *J. Geophys. Res.* **110,** B11105, doi:10.1029/2005JB003763 (2005).
12. White, R. S. *et al.* iSIMM pushes frontiers of marine seismic acquisition. *First Break* **20,** 782–786 (2002).
13. Roberts, A. W., White, R. S., Lunnon, Z. C., Christie, P. A. F., Spitzer, R. & iSIMM Team. In *Petroleum Geology: North-West Europe and Global Perspectives—Proc. 6th Petroleum Geology Conf.* (eds A. G. Doré & B. A. Vining) 755–766 (Geol. Soc. London, 2005).
14. Smith, L. K., White, R. S., Kusznir, N. J. & iSIMM Team. In *Petroleum Geology: North-West Europe and Global Perspectives—Proc. 6th Petroleum Geology Conf.* (eds A. G. Doré & B. A. Vining) 947–956 (Geol. Soc. London, 2005).
15. Christeson, G. L., McIntosh, K. D. & Karson, J. A. Inconsistent correlation of seismic layer 2a and lava layer thickness in oceanic crust. *Nature* **445,** 418–421 (2007).
16. White, R. S. *et al.* Imaging and regional distribution of basalt flows in the Faroe-Shetland Basin. *Geophysical Prospecting* **51,** 215–231 (2003).
17. Mutter, J. C., Talwani, M. & Stoffa, P. L. Origin of seaward-dipping reflectors in oceanic crust off the Norwegian margin by subaerial sea-floor spreading. *Geology* **10,** 353–357 (1982).
18. Smallwood, J. R., White, R. S. & Staples, R. K. Deep crustal reflectors under Reydarfjördur, eastern Iceland: Crustal accretion above the Iceland mantle plume. *Geophys. J. Int.* **134,** 277–290 (1998).
19. Smallwood, J. R., Staples, R. K., Richardson, K. R., White, R. S. & FIRE Working Group. Crust generated above the Iceland mantle plume: from continental rift to oceanic spreading center. *J. Geophys. Res.* **104,** 22885–22902 (1999).
20. McBride, J. H., White, R. S., Smallwood, J. R. & England, R. W. Must magmatic intrusion in the lower crust produce reflectivity? *Tectonophysics* **388,** 271–297 (2004).
21. Parkin, C. J., Lunnon, Z. C., White, R. S., Christie, P. A. F. & iSIMM Team. Imaging the pulsing Iceland mantle plume through the Eocene. *Geology* **35,** 93–96 (2007).
22. Cox, K. G. A model for flood basalt vulcanism. *J. Petrol.* **21,** 629–650 (1980).
23. Sallarès, V., Charvis, P., Flueh, E. R., Bialas, J. & the SALIERI Scientific Party. Seismic structure of the Carnegie ridge and the nature of the Galápagos hotspot. *Geophys. J. Int.* **161,** 763–788 (2005).
24. White, R. S., McKenzie, D. & O'Nions, R. K. Oceanic crustal thickness from seismic measurements and rare earth element inversions. *J. Geophys. Res.* **97,** 19683–19715 (1992).
25. Bown, J. W. & White, R. S. Variation with spreading rate of oceanic crustal thickness and geochemistry. *Earth Planet. Sci. Lett.* **121,** 435–449 (1994).
26. Nielsen, T. K. & Hopper, J. R. Formation of volcanic rifted margins: Are temperature anomalies required? *Geophys. Res. Lett.* **29,** 2022, doi:10.129/2002GL015681 (2002).
27. Lunnon, Z. C., Christie, P. A. F. & White, R. S. An evaluation of peak and bubble tuning in sub-basalt seismology: modelling and results. *First Break* **21,** 51–56 (2003).
28. Maresh, J. & White, R. S. Seeing through a glass, darkly: strategies for imaging through basalt. *First Break* **23,** 27–32 (2005).
29. Zelt, C. A. & Barton, P. J. Three-dimensional seismic refraction tomography: a comparison of two methods applied to data from the Faeroe Basin. *J. Geophys. Res.* **103** (B4), 7187–7210 (1998).
30. Zelt, C. A. & Smith, R. B. Seismic traveltime inversion for 2-D crustal velocity structure. *Geophys. J. Int.* **108,** 16–34 (1992).

Supplementary Information is linked to the online version of the paper at www.nature.com/nature.

Acknowledgements iSIMM was supported by Liverpool and Cambridge Universities, Schlumberger Cambridge Research Ltd, Badley Geoscience Ltd, WesternGeco, Amerada Hess, Anadarko, BP, ConocoPhillips, ENI UK, Statoil, Shell, the Natural Environment Research Council and the Department of Trade and Industry. OBSs were provided by Geopro GmbH and Q-Marine streamer acquisition by WesternGeco.

Author Contributions Wide-angle seismic analysis was undertaken by L.K.S. and A.W.R. as part of their PhD research. Seismic reflection processing for Fig. 2c was by WesternGeco. R.S.W. led the work at sea on RRS *Discovery* on the Faroes profile, N.J.K. on the Hatton profile, and P.A.F.C. oversaw the Faroes seismic profiling on MV *Geco Topaz*. R.S.W. wrote the paper and all authors discussed the results and commented on the manuscript.

Author Information Reprints and permissions information is available at www.nature.com/reprints. Correspondence and requests for materials should be addressed to R.S.W. (rwhite@esc.cam.ac.uk).

The iSIMM team includes, in addition to the other authors: A. M. Roberts[4], D. Healy[5], R. Spitzer[6], A. Chappell[5], J. D. Eccles[6], R. Fletcher[5], N. Hurst[5], Z. Lunnon[6], C. J. Parkin[6] & V. J. Tymms[5]

[4]Badley Technology Ltd, North Beck House, North Beck Lane, Hundleby, Spilsby, Lincolnshire PE23 5NB, UK. [5]Department of Earth Sciences, University of Liverpool, Liverpool L69 3BX, UK. [6]Bullard Laboratories, University of Cambridge, Madingley Road, Cambridge CB3 0EZ, UK.

METHODS

Wide-angle OBS data processing. The first data reduction step was to apply a drift correction to the internal OBS clocks, assuming a constant drift rate between the clock calibrations made immediately before deployment and after recovery: the average OBS clock drift rate was ~12 ms per day. Individual 60 s traces were then cut from the continuously recorded data for each of the four components (the vertical, two horizontal geophones, and the hydrophone), from every shot, with zero time at the shot instant. The next step was to calculate the position of the OBSs because some instruments drifted to an average distance of 400 m offline as they sank to the sea floor. For most of the OBSs this location was calculated using the direct water wave travel time at the point of closest approach, together with the water-wave acoustic velocity derived from the velocimeter dip and disposable bathy-thermographs. We assumed that the off-line water depth was identical to the on-line depth at the point of closest approach. For OBSs in the vicinity of crossover lines, where off-line shots were recorded, we were also able to locate the OBSs by triangulation. During the two-dimensional tomographic inversion modelling we assumed that the OBSs were positioned on the lines at the points of closest approach. Errors introduced by this procedure can be ignored for basalt or basement arrivals at offsets greater than 4 km, and are small compared to picking uncertainties. For the sediment velocities, we used move-out analysis on the coincident multichannel profile, so they are unaffected by this procedure.

No further processing was applied to the OBS data, other than de-meaning to remove small offsets and application of a 2–15 Hz band-pass zero-phase filter to attenuate noise outside this frequency range. It was possible to pick clear crustal diving phases (P_g) and Moho reflections (PmP) from almost all the OBSs on all the profiles, but mantle refractions (P_n) were apparent on only some of the OBSs. Uncertainties in the travel times were attached to each arrival pick according to the signal-to-noise ratio, varying from 10 ms for the best arrivals to 120 ms for the poorest, where it was possible that the correct first arriving phase had been missed, resulting in a cycle skip. Reciprocity tests were made to check the consistency of travel times between pairs of shotpoints and OBSs[30], and arrival picks were re-assessed where there was a significant discrepancy.

Tomographic velocity modelling. The velocity structure of the sediment section was derived by move-out analysis from the multichannel streamer data (12,000 m maximum offset on the Faroes profile, 2,400 m on the Hatton profile), because the 25 m group spacing of the processed streamer data provided better resolution than the OBS wide-angle data, which had a trace spacing of 75–100 m. A first two-dimensional inversion of the upper crustal structure was then calculated with the FAST program[29] using the travel times of first-arrival diving waves. Because diving waves are generally turned back in the upper half of the crust (see Supplementary Figs 2 and 5), this inversion constrained only the upper crustal structure well. The velocity model from FAST was used as the input for ray-tracing inversion using the computer program rayinvr[30]. Because rayinvr was used to invert for the arrival times of both the diving waves and the Moho reflections, this enabled us to construct whole-crustal two-dimensional models from the seabed to the base of the crust. The velocity structure was adjusted working downwards from the shallowest to the deepest crust by a combination of manual intervention to update the velocity structure and automatic inversions of specified single layers until the model-predicted arrival times were within the uncertainty of the data picks (that is, $\chi^2 \approx 1$). Finally, an automatic joint inversion of the diving waves and reflections was made using the tomo2D code[4], with the output from the rayinvr modelling used as the starting model. Decisions about the optimum parameters to use in construction of the models and smoothing during the inversion updates were made as in refs 31–33. The final model shown for the Faroes profile in Figs 3b, c was stopped at the stage of rayinvr ray-tracing rather than tomo2D inversion because the latter does not handle low-velocity zones well in its automatic procedure.

By design, the wide-angle velocity modelling was carried out largely independently of the reflection profile interpretation, so as to avoid bias in the model building. However, because the reflection profiles provided superior resolution in the sediment section, the structure and velocities of the sediments were derived from the reflection profiles as described above, and the shape of the prominent top–basalt interface at the base of the sediments was also determined from the reflection profiles. These constraints were used in the wide-angle modelling.

Estimates of the uncertainties in seismic velocities and interface depths and the resolution in the final models were made from a range of standard tests, including checker-board tests and a variety of ray density tests. We also tested the uncertainty of the final models by running to conclusion up to 100 different inversions for each profile with a range of randomized starting velocity models constrained by appropriate geological values for depth and velocity, and then calculating the standard deviation in velocity at every grid point and Moho depth along the profiles from the resultant array of output models. In general, the crustal velocities are constrained to better than 0.1 km s^{-1} and Moho depths to within 1 km (see Supplementary Figures for examples of the model uncertainties, and reports on the individual profile modelling[31–33] for further details).

31. Parkin, C. J. *Crustal Formation and the Influence of a Mantle Plume Following Continental Breakup of the Northern North Atlantic*. 1–225, PhD dissertation, Univ. Cambridge (2006).
32. Roberts, A. W. *Crustal Structure of the Faroes North Atlantic Margin from Wide-Angle Seismic Data*. 1–230, PhD dissertation, Univ. Cambridge (2007).
33. Smith, L. K. *Crustal Structure of Hatton Bank Volcanic Continental Margin from Traveltime Inversion of Wide-Angle Data*. 1–227, PhD dissertation, Univ. Cambridge (2006).